AIAA JOURNAL
Vol. 48, No. 11, November 2010

Experimental Investigation of a High-Lift Low-Pressure Turbine Suction Surface

Mark McQuilling* and Mitch Wolff†
Wright State University, Dayton, Ohio 45435
Sergey Fonov‡ and Jim Crafton§
Innovative Scientific Solutions, Dayton, Ohio 45440
and
Rolf Sondergaard¶
U.S. Air Force Research Laboratory, Wright–Patterson Air Force Base, Ohio 45433

DOI: 10.2514/1.37579

This work employs a shear and stress sensitive film (S3F) to investigate the suction surface flow features associated with a higher-lift low-pressure turbine airfoil (L2F). Well-behaved higher-lift low-pressure turbine designs suffer from an inability to accurately predict the transition location above the suction surface, and the separation onset locations obtained with the S3F sensor herein allow the validation of the separated-flow transition model used in the L2F design cycle. Improvements to the S3F measurement technique are explained in this work, and results are compared over a range of Reynolds numbers at 3.3% freestream turbulence including skin friction measurements at the trailing edge of the airfoil. Results demonstrate an improvement to the S3F data reduction process by accounting for the tunnel and model vibration, which will allow a greater range of sensor application.

Nomenclature

G	=	matrix of Green's functions
g	=	applied loads on film
p	=	pressure
PI	=	Coles' law of the wake pressure gradient parameter
r	=	film displacements
Re	=	inlet chord Reynolds number
v	=	streamwise velocity
v^+	=	velocity wall coordinate
v^*	=	friction velocity
x	=	streamwise coordinate
y	=	surface normal direction
y^+	=	surface normal wall coordinate
Zw	=	Zweifel loading coefficient

Greeks

δ	=	boundary layer height
ϵ	=	film deformations
η	=	kinematic viscosity of fluid
θ	=	volume deformation
λ	=	Lame constant
μ	=	film shear modulus
ν	=	film Poisson ratio
ρ	=	fluid density
τ_w	=	wall shear stress

Presented as Paper 2008-0079 at the 46th AIAA Aerospace Sciences Meeting and Exhibit, Reno, NV, 7–10 January 2008; received 16 March 2008; revision received 6 August 2010; accepted for publication 19 August 2010.

*Ph.D. Student; currently Assistant Professor of Aerospace and Mechanical Engineering, Saint Louis University, 3450 Lindell Boulevard, St. Louis, MO, 63103. Member AIAA.
†Professor, Mechanical and Materials Engineering, 3640 Colonel Glenn Highway. Associate Fellow AIAA.
‡Senior Scientist, 2766 Indian Ripple Road. Member AIAA.
§Scientist, 2766 Indian Ripple Road. Member AIAA.
¶Aerospace Engineer, Propulsion Directorate, 1950 Fifth Street. Member AIAA.

I. Introduction

THE design of efficient, high-lift low-pressure turbine (LPT) airfoils has been plagued by an inability to accurately predict the transition location along the suction surface. Locating transition has been cited as the major obstacle to overcome in order to obtain higher-lift LPTs which can mitigate the current low-Reynolds lapse in efficiency [1]. This lapse in performance as Reynolds number is decreased occurs primarily due to the flow separation which develops under the presence of an adverse pressure gradient on the suction surface [2]. Recently, Praisner and Clark developed a separated-flow transition model by examining 47 separated-flow with turbulent reattachment experimental test cases using actual turbine geometries [3]. This model was intended for Reynolds-averaged Navier–Stokes (RANS) computational fluid dynamics (CFD) solvers with sufficient accuracy for use in airfoil design systems, and was developed in conjunction with an attached-flow transition model based on 57 experimental test cases. The separated-flow model is a correlation relating the momentum thickness Reynolds number at separation onset to the length along the separation bubble to transition onset. The attached-flow model was cast into a critical relationship between a boundary layer diffusion time and the turbulent eddy length scale. Their separated-flow transition model was then used to design an LPT airfoil (L2F) with higher loading ($Zw = 1.59$) than any previously published design [4]. In addition to reducing the required airfoil count by 38%, the L2F airfoil exhibits an improved low-Reynolds performance over an LPT representative of those currently in service today (Pack B).

To validate the separated-flow transition model, the location of separation onset must be measured. Common techniques used to obtain separation onset information include pressure taps or transducers, but these techniques only provide pressure information at discrete locations along the surface which lend themselves well to instrumentation complexities. If separation occurs in between tapped locations, interpolations must be used which add unnecessary uncertainty into the onset location. Pressure-sensitive paints (PSPs) have also been used to provide a global pressure measurement, but its

limited dynamic range precludes the technique's use in low-speed aerodynamic testing [5]. Since the wall shear stress is zero at the separation onset location [6], skin friction measurement techniques can also be employed to determine separation onset locations. Liquid crystals applied to the test surface can provide a global skin friction measurement, but typically require a complicated application and calibration process and have the need for a new coating after each test run [7]. Crystal roughness effects on the flow also preclude their use in the low-Reynolds flow regime. Another global sensor using a thin elastomer film to measure skin friction was developed in the early 1990s as a direct method to measure surface shear forces [8]. This technique relied on an interference method to track the response of the film due to an applied load, and the shearing stress which caused the shear deformations were determined from Hooke's Law for shear strain. The thin elastomer film approach was further refined in order to provide two-dimensional static pressure measurements without the drawbacks of PSPs such as the need for oxygen in the flow environment and the limited pressure sensitivity, dynamic range, and frequency response [5]. The resulting shear and stress sensitive film, or S3F, provides a simultaneous measurement of static pressure and skin friction obtained with the use of a single charge-coupled device (CCD) camera.

The current study investigates the suction surface of a high-lift LPT airfoil (L2F) with a nominal Zweifel loading coefficient of 1.59 [4]. Shear stress measurements are acquired in the leading-edge and the trailing-edge regions of the airfoil using the S3F shear and stress sensitive film. Previous work has shown the ability of S3F to be applied to an LPT surface [9], and this study continues the development of the technique in the low flow speed range while providing separation onset locations necessary for the validation of the separated-flow transition model used in the L2F design [4]. The improved data reduction routine is also explained in this work. Two separate rounds of S3F results on the trailing-edge region for identical flow conditions showcase the improvement in S3F data reduction over the course of this work. Thermal anemometry is also used to acquire mean velocity profiles along the latter portion of the airfoil, and shear stress determined by matching turbulent similarity profiles is compared with the shear stress obtained with the S3F sensor in order to provide a measure of the accuracy of the technique in the low-Reynolds flow regime.

II. Experimental Arrangement

All tests were conducted in the low-speed wind tunnel (LSWT) of the Air Force Research Laboratory (AFRL) at Wright–Patterson Air Force Base in Dayton, Ohio. The LSWT is powered by a 125-hp electric motor driving an axial fan located downstream of the 0.85 by 1.22 m clear polycarbonate test section. The 3.0 by 2.7 m rectangular bell-mouth inlet is followed by honeycomb flow straighteners and a gradual 8:1 area contraction. The full view can be seen in Fig. 1a and a top view of the test section with an eight-blade turbine cascade is in Fig. 1b. Adjustable tailboards maintain periodicity across the cascade and can be angled to allow various inlet and exit angles. Turbulence is generated 2.3 m upstream of the test section with a square-mesh array grid of 2.54 cm diameter tubes spaced 7.6 cm apart, producing 3.3% freestream turbulence. For a Reynolds number of 25,000, the grid produces an integral length scale of 3.51 cm, a Taylor microscale of 0.38 cm, and a Kolmogorov length scale of 0.08 cm at the entrance to the cascade. At $Re = 75,000$, these scales are 4.19, 0.81, and 0.05 cm, respectively. Inlet flow diagnostics include a thermocouple, hot-wire, and pitot-static tube. Four 1.5 m long traverse slots are located atop the test section both upstream and downstream of the cascade, and a three-axis traverse mounted on top of the test section can measure a planar section of the wind tunnel through these slots. A smaller three-axis traverse can be placed inside the tunnel and is accurate to within ± 0.01 mm; this smaller traverse is used to position the hot-film probe in the boundary layer of the L2F cascade.

The L2F linear turbine cascade was fitted with 7 airfoils having an axial chord of 6 in to achieve periodicity. All results presented herein are taken on the middle blade in the passage. The airfoils have a 0.876 m span, an inlet angle of 35 deg and an exit angle of 60 deg. The L2F was designed using RANS flow solver [10] with a separated-flow transition model [3] and an algebraic turbulence model [11]. The L2F with nominal Zweifel equal to 1.59 exhibits an improved Reynolds lapse characteristic and 38% higher lift than the Pack B [4], an LPT representative of those currently in service today.

Thermal anemometry measurements were acquired with an eight-channel IFA 300 constant temperature anemometer made by TSI connected to a PC through a National Instruments PXI-1010 chassis with 16 bit analog/digital conversion. Velocity profiles presented in this work were obtained using a single normal hot-film (model 1211-20) manufactured by TSI. Each data point taken with the 3.2 mm long, 0.5 mm diameter hot-film was acquired at 50 kHz for 250,000 samples. Reimann et al. have previously used hot-film anemometry to describe the turbulent character of separated flow above the Pack B and L1M airfoils [12], providing information such as locations of separation onset, transition onset and length, turbulent reattachment, and intermittency (percentage of time the flow is turbulent). An intermittency of one denotes a turbulent flow while an intermittency of zero indicates a laminar flow. In this work, an intermittency algorithm is used which was originally developed for tracking the leading and trailing edges of turbulent spots using surface-mounted heat-flux gauges [13], and has been found to work equally as well defining transition and turbulence above the surface [4]. This algorithm is used to determine where transitional and turbulent velocity profiles occur along the surface of the L2F airfoil. Turbulent profiles determined in this manner are compared for turbulent similarity to Coles' Law of the Wake [14] given by Eq. (1):

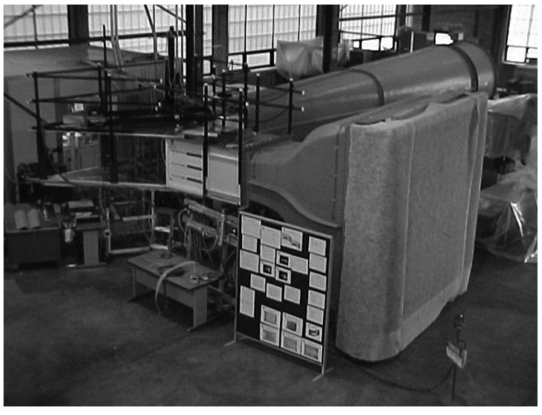

a) Full view

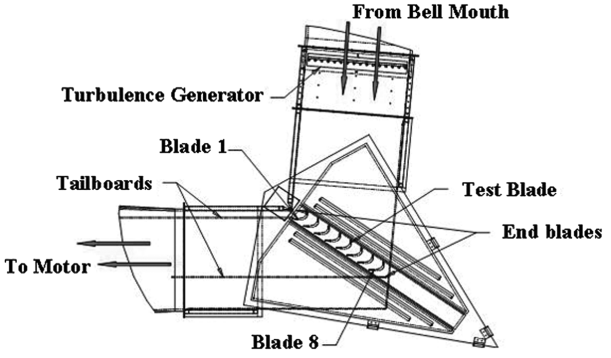

b) Test section top view, Pack B cascade

Fig. 1 AFRL's LSWT.

$$v^+ = \frac{1}{\kappa}\ell_n(y^+) + B + \frac{2PI}{\kappa} f\left(\frac{y}{\delta}\right) \tag{1}$$

Here, κ is the von Kármán constant equal to 0.41 and B is set to 5.0. The PI term accounts for the pressure gradient, δ is the boundary layer thickness, and v^+ and y^+ are the wall coordinates given by

$$v^+ = \frac{v_{\text{mean}}}{v^*} \qquad y^+ = \frac{yv^*}{\eta} \tag{2}$$

where v^* is the friction velocity defined as

$$v^* = \sqrt{\frac{\tau_w}{\rho}} \tag{3}$$

with τ_w being the wall shear stress and ρ the density of the fluid. During the course of this study it was found that the boundary layer thickness, δ, was more consistently determined by tracking the location of 99% freestream velocity rather than the location where the partial derivative of u with respect to the wall-normal direction goes to near zero. To match the turbulent profiles, the wall shear stress and PI term are iterated upon until a best-fit occurs over the appropriate wall coordinate range. The last term in Eq. (1) includes a function of surface normal height approximated by

$$f\left(\frac{y}{\delta}\right) = 3\left(\frac{y}{\delta}\right)^2 - 2\left(\frac{y}{\delta}\right)^3 \tag{4}$$

This function produces the S shape experienced by turbulent boundary layer profiles under the influence of an adverse pressure gradient [14]. Turbulent similarity comparisons are used in this work to provide an independent value of surface shear to compare with the S3F sensor.

The S3F shear and stress sensitive film uses a polymeric film impregnated with luminescent molecules and doped with tracer particles on its surface which adhere to the surface under a load but do not alter the surface roughness characteristics of the film, as described in detail by Fonov et al. [5]. The film is created using a shallow cavity filled with the S3F material which polymerizes and behaves like an incompressible fluid. Upon application of a force, the film deforms in both normal and tangential directions but does not compress. The luminescent molecules are excited by a light-emitting diode (LED) lamp at one wavelength and emit at another wavelength recorded by a CCD camera. The intensity of the emission is proportional to the thickness of the film, providing a normal deformation measurement. This type of thickness measurement requires a stable light source and at least a 12-bit CCD camera. Both a flow-off and flow-on image are required to record the changes due to the flow, making the S3F sensor a differential gage between two conditions. The streamwise and spanwise displacements of the film are determined by spatially cross-correlating the flow-on and flow-off images of the surface providing a two-component displacement map. Thus, all three components of deformation are recorded by a single high-resolution camera. The typical S3F data acquisition system is shown in Fig. 2. Although great care is taken to ensure the highest stability of all signal acquisition and processing equipment, variations still occur. In addition to the flow-on and flow-off images, the data reduction requires a background image to be acquired with no wind forces or lighting. The reduction process removes the signal contributions of the background and flow-off fields. The differential nature of the technique also provides a means to cancel other sources of error such as unequal illumination intensity across the surface, uneven luminophore dispersion, uneven acquisition across the CCD sensor, or temperature variation across the measured surface. The dynamic range can be tuned by chemically modifying the film's modulus of elasticity and Poisson ratio. The normal pressure and tangential surface stresses which caused the three-dimensional deformations are determined from an inverse finite element model [9], whose inputs are the film's emission intensity and the tracer translations between flow-off and flow-on conditions. Accuracy of the technique depends on stability of the illumination and detector electronics, as well as the existing background electrical and

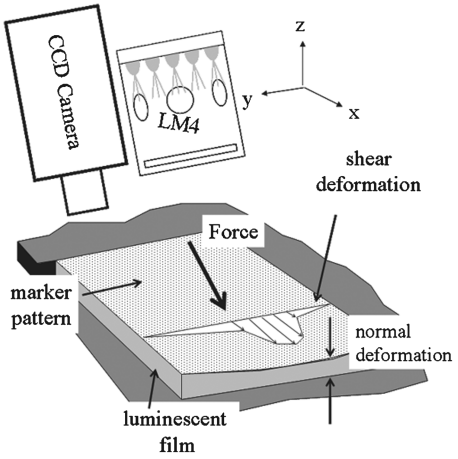

Fig. 2 S3F data acquisition system.

magnetic fields in the location where data is acquired. For the films used and displacements measured in this work, the uncertainty in thickness measurement and shear modulus are 2% each, while uncertainty in displacement is 6%. Therefore the total uncertainty in the force measurements with the current data reduction is 10%. In this work, the suction surface of the L2F airfoil is illuminated with an Innovative Scientific Solutions, Incorporated (ISSI) LM4 LED lamp and detected by a 14-bit PCO.1600 CCD camera with 1600×1200 pixel resolution using a 50 mm lens. The camera used in these experiments was specifically selected for its stability, and is colocated with the LED lamp approximately 0.75 m away from the model surface. The LED illuminator was custom designed and constructed at Innovative Scientific Solutions, Inc., with stability of emission intensity as a key performance parameter. The luminophore was selected for emission intensity at specific dynamic ranges, and has a response time of 10 ms. A single low-pass filter is used to distinguish the fluorescent emission while an ISSI timing box controls the excitation-detection sequence. Data is collected and stored on a PC.

The data reduction process for the S3F sensor in the current work has been improved beyond a previous publication [9] to assist determination of the error in the measurement. All steps are identical as before until the Lame system of equations are solved. The following details how the error functions are determined during data reduction for a two-dimensional case. The Lame system of equations for a two-dimensional case can be rewritten as

$$\begin{aligned} \mu\nabla^2 u_x + (\lambda+\mu)\frac{\partial}{\partial x}\left(\frac{\partial u_x}{\partial x} + \frac{\partial u_y}{\partial y}\right) = 0 \\ \mu\nabla^2 u_y + (\lambda+\mu)\frac{\partial}{\partial y}\left(\frac{\partial u_x}{\partial x} + \frac{\partial u_y}{\partial y}\right) = 0 \end{aligned} \tag{5}$$

where $\nabla^2 = (\frac{\partial^2}{\partial x^2} + \frac{\partial^2}{\partial y^2})$ and using pressure $p = \lambda(\frac{\partial u_x}{\partial x} + \frac{\partial u_y}{\partial y})$. For noncompressible S3F corresponding to $\lambda \to \infty$ and $\nu \to 0.5$, this system can be presented as

$$\mu\nabla^2 u_x + \frac{\partial p}{\partial x} = 0 \tag{6}$$

$$\mu\nabla^2 u_y + \frac{\partial p}{\partial y} = 0 \tag{7}$$

The boundary conditions are $u = 0$, excluding the contact surface S where the surface pressure p and friction f are

$$p = \lambda\left(\frac{\partial u_x}{\partial x} + \frac{\partial u_y}{\partial y}\right)_S \qquad f = \mu\left(\frac{\partial u_x}{\partial y} + \frac{\partial u_y}{\partial x}\right)_S \tag{8}$$

Let us consider several solutions of system (6) and (7) in the region far away from left and right boundaries:

1) Displacement field is $u_x = c_1 y$; $u_y = 0$ will correspond to action of the pure friction force $f = c_1 \mu$ on contact surface S and shear displacement component:

$$u_x(x, h) = \frac{h}{\mu} f \tag{9}$$

2) Displacement component $u_x = c_1 y h(1 - y/2h)$ and $u_y \ll u_x$ will satisfy Eq. (6) if $\frac{\partial p}{\partial x} = \frac{c_1}{\mu} =$ constant. Surface shear displacement component will be proportional to pressure gradient and can be treated as cross talk between normal tension and shear displacement:

$$u_x(x, h) = \frac{h^2}{2\mu} \left(\frac{\partial p}{\partial x} \right)_S \tag{10}$$

3) Displacement components $u_x(x, y) = c_1 xy$ and $u_y(x, y) = c_2 y^2$ will satisfy Eqs. (6) and (7) if the surface friction has constant gradient $\frac{\partial f}{\partial x} = c_i \mu$ and $c_2 = -c_1/2$. Reaction in normal direction on shear gradient on the contact surface S will be

$$u_y(x, h) = \frac{-h^2}{2\mu} \left(\frac{\partial f}{\partial x} \right)_S \tag{11}$$

Again it can be treated as cross talk between shear tension and normal displacement.

4) Displacement field

$$u_x(x, y) = c_{1x} \left(1 - \frac{y}{2h} \right) xy, \qquad u_y(x, y) = c_{1y} \left(1 - \frac{y}{3h} \right) y^2$$

will be created by surface pressure field having constant second derivative, that is $\frac{\partial^2 p}{\partial x^2} = c_{1x} \frac{\mu}{h}$, zero friction force, and $c_{1x} = -c_{1y}$ that follows from zero-compressibility of S3F. Normal component of surface displacement can be expressed as

$$u_y(x, h) = -\frac{h^3}{3\mu} \left(\frac{\partial^2 p}{\partial x^2} \right)_S \tag{12}$$

and shear component

$$u_x(x, h) = \frac{h^2 x}{2\mu} \left(\frac{\partial^2 p}{\partial x^2} \right)_S \tag{13}$$

which is zero at $x = 0$ and $\langle u_x(x, y) \rangle_{-L/2, L/2} = 0$ on the interval $[-L/2, L/2]$. The total surface displacement can be treated as the superposition of these four cases:

$$u_x(x, h) = \frac{h}{\mu} \left(f + \frac{h}{2} \frac{\partial p}{\partial x} \right)_S \tag{14}$$

$$u_y(x, h) = -\frac{h}{\mu} \left(\frac{h}{2} \frac{\partial f}{\partial x} + \frac{h^2}{3} \frac{\partial^2 p}{\partial x^2} \right)_S \tag{15}$$

Equations (14) and (15) are valid only for loads with low spatial frequency content. Using Gauss-type load distribution like $p(x, d) = \exp(-(x/d)^2)$, it is possible to estimate the error of this model as a function of spatial frequency bandwidth which is $\Delta\Omega \approx h/d$ in this case. Let us introduce new dimensionless variables:

$$\tilde{p} = p/\mu, \qquad \tilde{f} = f/\mu, \qquad \tilde{x} = x/h$$

Equations (14) and (15) can be rewritten as

$$\tilde{u}_x(\tilde{x}, 1) \approx \left(\tilde{f} + \frac{1}{2} \frac{\partial \tilde{p}}{\partial \tilde{x}} \right)_S + O(\tilde{f} \cdot \mathrm{err}_{xx}(\Delta\Omega) + \tilde{p} \cdot \mathrm{err}_{yx}(\Delta\Omega)) \tag{16}$$

$$\tilde{u}_y(\tilde{x}, 1) \approx -\left(\frac{1}{2} \frac{\partial \tilde{f}}{\partial \tilde{x}} + \frac{1}{3} \frac{\partial^2 \tilde{p}}{\partial \tilde{x}^2} \right)_S + O(\tilde{f} \cdot \mathrm{err}_{xy}(\Delta\Omega) + \tilde{p} \cdot \mathrm{err}_{yy}(\Delta\Omega)) \tag{17}$$

Functions $\mathrm{err}(\Omega)$ were estimated using finite element analysis (FEA) and presented in Fig. 3.

III. Results

The S3F tests conducted at AFRL were completed in two rounds; the first placed separate patches of S3F for the leading and trailing edges, and the second round placed one continuous patch from the trailing edge to nearly 42% of the suction surface length (SSL). Round 1 results were intended to check the formulations of the S3F sensor and make sure the stiffness was properly selected for the local stress levels. The separation onset locations near the L2F leading edge obtained from the round 1 results were used in the validation of the separated-flow transition model used for the L2F design [4]. Round 2 examines the trailing-edge region with another S3F patch, and these results are compared with the round 1 trailing-edge data to gain more insight into the data reduction process, thus helping ISSI obtain a better feel for the film's performance over two test points with the same flow conditions. Obtaining results with S3F in these low flow speeds is still a challenging task, as round 1 produces different magnitude friction forces on the trailing edge than round 2. In fact, the friction patterns are also different.

Figure 4 presents round 1 S3F results for the leading-edge region of the L2F blade. These results cover approximately 5 to 35% SSL. Figures 4a–4c show the displacement maps with streamlines showing surface friction direction, and are oriented with the flow coming from the right and going to the left (camera point of view). These figures show the L2F blade indeed separates, as the nodal line of separation can be seen for all three Re where the downstream (left) facing vectors converge with the upstream (right) facing vectors on the left side of the plots. These closed nodal separations are seen to originate and terminate with saddle points which typically represent locations of increased vorticity above the surface [15]; it is unclear, however, if these saddle points are representative of true L2F flow physics or are caused by the S3F patch's spanwise edge. The $Re = 25k$ case shows a separation line which is a function of airfoil span (y-direction), indicating an unsteady separation onset location which is influenced by the edge of the S3F patch. The other two Re maps display a separation line more consistent with span, and is located slightly further downstream than $Re = 25k$. At $Re = 75k$ in Fig. 4c, we also notice an additional pair of nodal separation and reattachment lines on the bottom half of the figure which collapse into the saddle point near midplot. Figure 4d presents the information which will be used in validating the separated-flow transition model. This

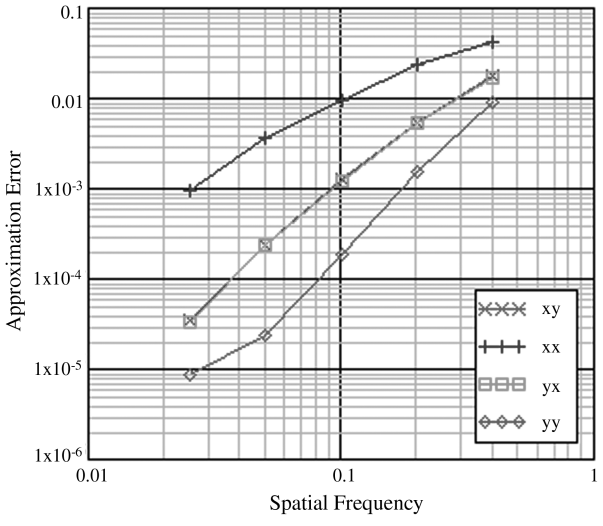

Fig. 3 FEA estimation of errors function $\mathrm{err}_{xxyy}(\Delta\Omega)$.

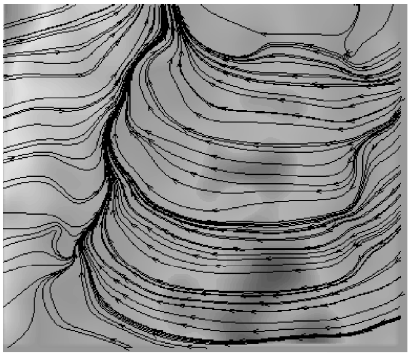

a) *Re* = 25*k*, flow right to left

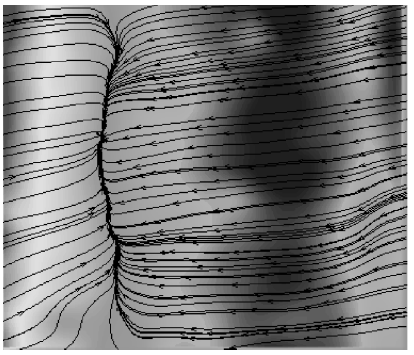

b) *Re* = 50*k*, flow right to left

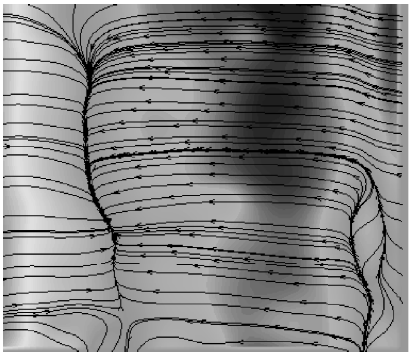

c) *Re* = 75*k*, flow right to left

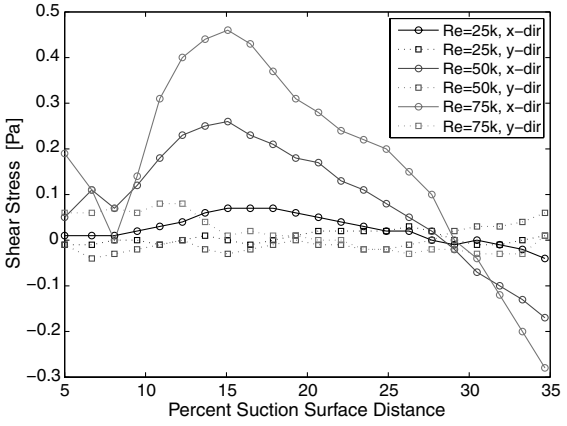

d) Composite

Fig. 4 S3F round 1: force distributions near L2F leading edge, 5–35% SSL, flow left to right.

figure presents the streamwise (x-direction) and transverse (y-direction) surface shear results averaged over the span for the maps presented in Figs. 4a–4c. Here the flow is coming from the left going to the right, so positive friction is directed downstream and negative friction is directed upstream, indicating the reverse flow inside of a separation bubble. The small magnitude transverse friction (y-dir) indicates a mostly two-dimensional flow for all three Reynolds numbers with slight variation possibly due to the unsteady nature of separation bubbles. The streamwise surface shear (x-direction) for $Re = 25k$ indicates a separation at approximately 26% SSL where the friction changes sign from positive (downstream) to negative (upstream). This location will be used later to validate the separated-flow transition model, where the model information will be taken from the nearest available boundary velocity profile location of 25.2% SSL. Increasing Re moves this separation location slightly further downstream, where the $Re = 50k$ case is just upstream of the $75k$ case. Model validation for these two latter cases will require boundary information from their nearest available profile, both selected as 28.0% SSL. Also as expected in this figure we see that friction is proportional to Reynolds number as the friction peak for the leading edge, which remains near 15% SSL, increases with Re as the faster oncoming flow impacts the surface with a greater load. Table 1 presents the experimental separation onset locations along with Wildcat CFD predictions in percent suction surface distance. Wildcat is a compressible Navier–Stokes flow solver used to design the L2F turbine airfoil [4]. Wildcat predictions occur further downstream than those found by experiment, although the proximity of the two methods is encouraging.

Table 1 L2F separation onset locations, % SSL

Method	$Re = 25k$	$Re = 50k$	$Re = 75k$
S3F	26.0	28.0	28.0
Wildcat[a]	27.5	29.0	29.0

[a]Wildcat CFD predictions from L2F design [4].

Figure 5 presents the round 1 streamwise S3F results for all three Re from 67% SSL to the trailing edge of the L2F airfoil along with shear stress estimates from matching turbulent velocity profiles to Coles' law of the wake for 82 and 90.4% SSL at $Re = 50$ and $75k$. Again the flow is left to right, so a positive shear stress indicates downstream flow while a negative stress indicates upstream flow (separation). This figure shows the friction forces experienced in this flow at the trailing edge are less than 1 Pascal. We also see that the $Re = 25k$ and $50k$ cases are separated by the beginning of the patch, and both reattach near 92–94% SSL. It is not clear whether or not the separation noticed here is continued from the leading edge or if it is caused by a disturbance of the film's upstream edge. The $Re = 75k$ case appears attached as the patch begins, signalling that the

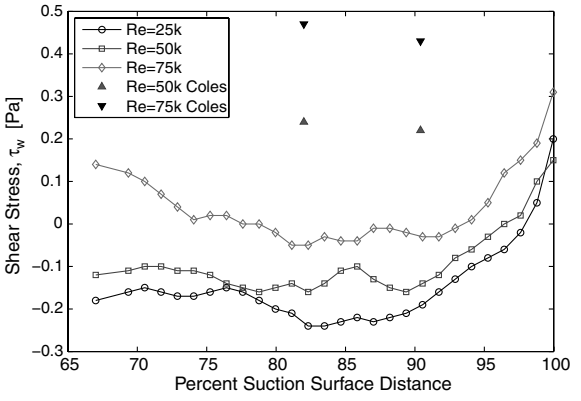

Fig. 5 S3F round 1: force distributions near L2F trailing edge, 67–100% SSL.

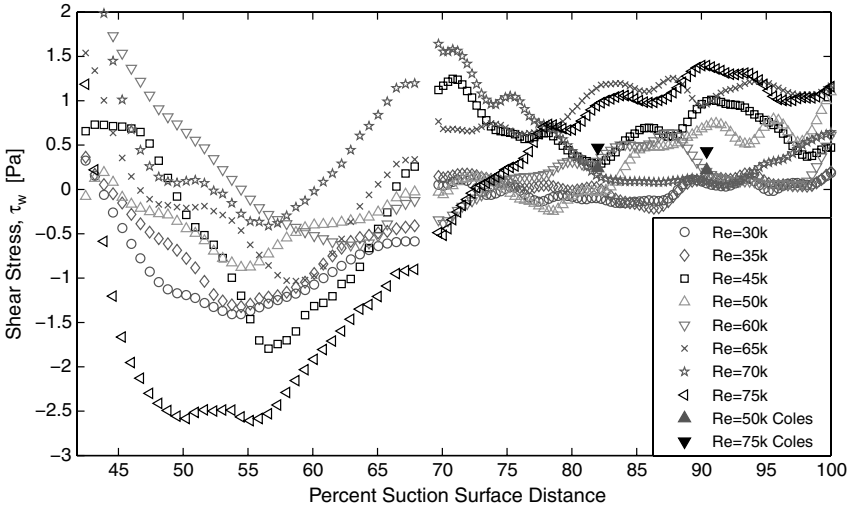

Fig. 6 S3F round 2: friction force distributions on L2F, flow left to right, 41.8–100% SSL.

separation near 28% SSL must have reattached somewhere before 67% SSL. The flow again briefly separates near 77% SSL only to reattach before the end of the blade near 92% SSL. Comparing the shear estimates from velocity profiles to S3F results shows the difficulty in resolving such low shear stress near 1 Pascal, as all estimates are above the shear produced by the S3F sensor. This flow description will be contradicted by the round 2 results, again showing the difficulty experienced when resolving friction forces on the order of 1 or less Pascals, compounded with errors associated with model and tunnel movement. To reduce the round 1 S3F data, several marker patches are distributed on the S3F patch which provide a reference between the unloaded and loaded state. The total S3F displacement is a combination of the linear displacement caused by the true friction force, the rotations and linear displacements caused by the S3F response under a loaded state, and movement of the model itself, where even a few pixels of translation can cause significant error.

Figure 6 presents the second round of S3F results for the L2F airfoil using the single continuous patch on the latter portion of the airfoil. In this figure, two data sets have been combined into one global picture, each data set separated by a small distance in the middle of the plot. Breaking up the data set into two areas was necessary to maintain proper camera resolutions and focusing over the large patch covering a substantial length of the trailing-edge region. This figure shows time-averaged friction force distributions for the L2F airfoil over Reynolds numbers from 30 to 75k covering 41.8 to 100% SSL plotted along with the same shear estimates from turbulent velocity profile matching to Coles' law of the wake similarity profiles for 82 and 90.4% SSL. Again the flow is from left to right, so positive shear indicates downstream flow and negative shear indicates reverse flow in a separation bubble. During this round of S3F tests, it was initially found that the tunnel vibration induced inaccuracies in the data reduction due to excess pixel movement ($\sim$5 pixels). The sensitivity of S3F dictates that even a few pixels of model or tunnel movement registered by the CCD camera must be cancelled out in order to provide the most accurate results. To alleviate these problems, the camera and LED apparatus were bolted to the tunnel and marker dots were applied to the S3F patch as well as to the airfoil surface under the S3F patch, increasing the complexity of data reduction but providing a means to cancel model movement during the loaded condition. It should again be noted these round 2 results show a different flow pattern than the earlier round 1 results, a discrepancy which illustrates the reduction process still needs more development before accurate skin friction can be obtained at the air flow speeds encountered in this work; in fact, these test conditions may be at the boundary of the technique. The best approach to this point seems to be providing independent discrete measurement of surface shear at certain locations and then calibrating the S3F regional results to the discrete information.

Examining the right side of Fig. 6 shows similar trends over all Reynolds numbers but with varying shear magnitudes. For $Re=75k$, the round 2 results show higher wall shear than round 1. The magnitude remains near the same for round 1 and round 2 near $Re = 50k$, but neither $Re = 50k$ or $Re = 75k$ matches the surface shear estimates obtained from fitting Coles' law of the wake turbulent similarity velocity profiles. However, round 2 results are closer than round 1 results, indicating some improvement in result accuracy when accounting for tunnel and model movement during the data reduction process. The left side of Fig. 6 shows somewhat similar trends over varying Reynolds number for the region spanning 41.8 to 67.9% SSL, although different from round 1 results. All flow patterns experience a drop in friction which separates as shear changes from positive to negative. Although varying Re show an inconsistent trend in magnitude, the overwhelming pattern shows a region of decreasing shear which troughs between 50–60% SSL. The wall shear then recovers towards the downstream values near 67.9% SSL, although some Reynolds numbers exhibit better matching to downstream shear values than others. The waviness in all shear profiles, especially those downstream, indicates the elastic modulus of the S3F film may not be properly suited for all Reynolds numbers tested due to their varying frequency content. Since these test conditions appear to be at the boundary of the S3F technique, the sensitivity of elastic modulus to resolution accuracy may change significantly over the change in flow speeds encountered through the surveyed Reynolds numbers.

IV. Conclusions

The current study successfully used a shear and stress sensitive film to obtain separation onset locations on the L2F LPT airfoil consistent with previous CFD predictions. These onset locations helped validate the separated-flow transition model used during the L2F design cycle [4]. New composition films were developed for very low air flow speed testing, although two separate rounds of S3F tests over identical flow conditions resulted in different flow results, both in pattern and magnitude. The accuracy of the second round was improved, however, by accounting for errors induced by tunnel vibration and model movement into the data reduction process. These errors were cancelled by securing the CCD camera and LED apparatus onto the tunnel test section and by using additional marker strips located on the model adjacent to the S3F patch. Thus, the data reduction process was improved for low air flow speeds, which will allow a greater range of application for future S3F tests.

Acknowledgments

The first author wishes to thank the Dayton Area Graduate Studies Institute for financial support. All authors wish to thank Grant Jones

of Innovative Scientific Solutions, Inc., for developing the chemical compositions of the S3F sensor used during these tests.

References

[1] Wisler, D., "The Technical and Economic Relevance of Understanding Boundary Layer Transition in Gas Turbine Engines," Minnowbrook 2 1997 Workshop on Boundary Layer Transition in Turbomachines, NASA CP-1998-206958, 1998.

[2] Sharma, O., "Impact of Reynolds Number on LP Turbine Performance," Minnowbrook 2 1997 Workshop on Boundary Layer Transition in Turbomachines, NASA CP-1998-206958, 1998.

[3] Praisner, T. J., and Clark, J. P., "Predicting Transition in Turbomachinery, Part 1-A Review and New Model Development," *Journal of Turbomachinery*, Vol. 129, No. 1, 2007, pp. 1–13. doi:10.1115/1.2366513

[4] McQuilling, M., "Design and Validation of a High-Lift Low-Pressure Turbine Blade," Ph.D. Dissertation, Wright State Univ., Dayton, OH, Aug. 2007.

[5] Fonov, S., Goss, L., Jones, G., Crafton, J., Fonov, V., and Ol, M., "New Method for Surface Pressure Measurements," AIAA Paper 2005-1029.

[6] Schlichting, H., and Gersten, K., *Boundary Layer Theory*, 8th ed., Springer, New York, 2001.

[7] Plesniak, M. W., and Peterson, S. D., "Wall Shear Stress Measurements for Conventional Applications and Biomedical Flows (invited)," AIAA Paper 2004-2301.

[8] Tarasov, V. N., and Orlov, A. A., "Method for Determining Shear Stress on Aerodynamic Model Surface," Patent of Russia, 4841553/23/1990.

[9] McQuilling, M., Wolff, M., Fonov, S., Crafton, J., and Sondergaard, R., "An Experimental Investigation of a Low-Pressure Turbine Blade Suction Surface Using a Shear and Stress Sensitive Film," *Experiments in Fluids*, Vol. 44, No. 1, 2008, pp. 73–88. doi:10.1007/s00348-007-0375-2

[10] Dorney, D., and Davis, R., "Navier–Stokes Analysis of Turbine Blade Heat Transfer and Performance," *Journal of Turbomachinery*, Vol. 114, No. 4, 1992, pp. 795–806. doi:10.1115/1.2928033

[11] Baldwin, B., and Lomax, H., "Thin Layer Approximation and Algebraic Model for Separated Turbulent Flows," AIAA Paper 78-257.

[12] Reimann, D., Bloxham, M., Crapo, K., Pluim, J., and Bons, J., "Influence of Vortex Generator Jet-Induced Transition on Separating Low Pressure Turbine Boundary Layers," AIAA Paper 2006-2852.

[13] Clark, J., Jones, T., and LaGraff, J., "On the Propagation of Naturally-Occurring Turbulent Spots," *Journal of Engineering Mathematics*, Vol. 28, No. 1, 1994, pp. 1–19. doi:10.1007/BF02383602

[14] White, F., *Viscous Fluid Flow*, 3rd ed., McGraw–Hill, New York, 2006.

[15] Tobak, M., and Peake, D., "Topology of Three-Dimensional Separated Flows," *Annual Review of Fluid Mechanics*, Vol. 14, 1982, pp. 61–85. doi:10.1146/annurev.fl.14.010182.000425

K. Asai
Associate Editor